

Particle trapping via surface wave and bottom topography interactions

Akanksha Gupta^{1,2} and Anirban Guha³†

¹Environmental and Geophysical Fluids Group, Department of Mechanical Engineering, Indian Institute of Technology, Kanpur, U.P. 208016, India.

²Aix Marseille University, CNRS, Centrale Marseille, IRPHE (UMR 7342), Marseille 13384, France.

³School of Science and Engineering, University of Dundee, DD1 4HN, U.K.

(Received xx; revised xx; accepted xx)

Ocean surface waves cause floating particles to undergo a slow drift in the direction of propagation of the waves. This forward drift, commonly known as the Stokes drift, plays a crucial role in the transport of various tracer parcels, from sediments to pollutants, in the marine environment. We show that this drift is significantly affected when an incident surface wave travels over a small amplitude, corrugated sea-floor. The mechanism at work is Bragg resonance; reflected waves are generated via nonlinear resonant interactions between an incident wave and a rippled bottom. First, we theoretically explain the fundamental effect of two counter-propagating Stokes' waves on Stokes drift and then perform numerical simulation of Bragg resonance using High-order Spectral method. A monochromatic incident wave on interaction with a rippled patch of bottom topography yields a complex interference between the incident and reflected waves. When the velocity induced by the reflected waves exceeds that of the incident, particle trajectories reverse, leading to a backward drift. We observe that all parcels placed on the free surface above the patch are trapped, implying that the small amplitude rippled patch acts as a non-surface-invasive particle trap. These ideas may be useful for designing artificial, corrugated sea-floor patches for mitigating microplastics and other forms of ocean pollution. We also expect that naturally occurring sea-floor corrugations, especially in littoral zones, may significantly affect tracer transport in oceans.

Key words:

1. Introduction

Surface gravity waves existing at the ocean free surface cause floating particles, in addition to its periodic to-and-fro motion, a net transport in the direction of wave propagation, commonly known as the *Stokes drift* (Stokes 1847). While periodic motion arises from the velocity field set by the surface wave at the leading order (i.e. *linear* part of the wave's field), Stokes drift results from the second order effects of a weakly nonlinear wave (wave steepness is small but non-negligible). More specifically, Stokes drift is the difference between the wave-averaged velocity following a parcel (i.e. Lagrangian frame) and the average Eulerian flow velocity of the fluid (Van den Bremer & Breivik 2017; van Sebille *et al.* 2020). Even though Stokes drift is proportional to the square

† Email address for correspondence: anirbanguha.ubc@gmail.com

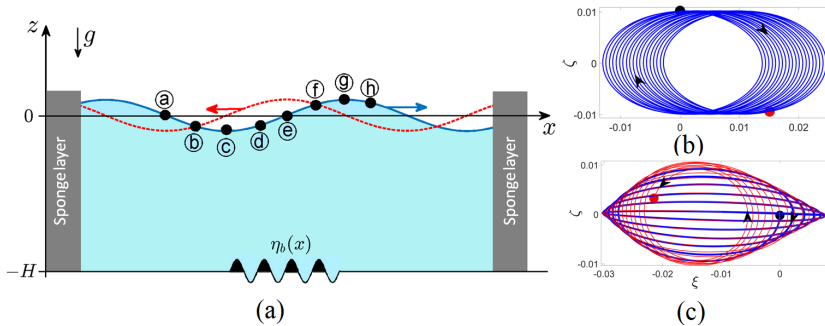


FIGURE 1. (a) Schematic of surface wave and bottom ripple with particles at different positions (labeled a–h) at $t = 0$. Interaction of the rightward propagating incident wave (deep blue curve centered at $z = 0$) with the bottom ripple (undulations centered at $z = -H$) leads to the generation of a leftward propagating reflected wave (red dashed curve centered at $z = 0$). In reality, many reflected waves are generated from a finite patch, but here just one is shown for simplicity. (b) Trajectory of a particle in the absence of bottom ripple, and (c) trajectory of particle labeled d in the presence of bottom ripple. In (b)–(c), black and red filled circles respectively denote initial and final location of the particle. Blue curves represent clockwise (forward) trajectories while red curves represent anti-clockwise (backward) trajectories.

of wave steepness (therefore a small quantity in comparison to the leading order orbital motions), its magnitude is still significant and has important consequences (McWilliams & Restrepo 1999). Moreover, Stokes drift can be inferred from high-frequency radar, has the potential to be estimated from satellite measurements, and has already been accurately measured in the laboratory (van Sebille *et al.* 2020, and references therein). The importance of Stokes drift in the transport of various types of marine particles cannot be overstated. It is known to play a key role in sediment transport (Santamaria *et al.* 2013), the local modelling of marine oil spills, significantly contributes to the trajectories of drifters, especially for search and recovery missions (crash of MH370), and is also significant in mapping the pathways of plastic pollution including microplastics in the global oceans (Van den Bremer & Breivik 2017; van Sebille *et al.* 2020, and references therein).

Studies on Stokes drift have primarily approximated the ocean bottom to be a flat surface, while in reality, ocean bottom topography is spatially varying. Seafloor variations, much like mirrors and lenses in optics, can significantly affect the propagation of incident waves (Elandt *et al.* 2014). An incident surface wave can interact with small undulations at the ocean bottom (hereafter, bottom ripple), giving rise to a reflected surface wave. This special type of wave-triad interaction is known as *Bragg resonance*; here the bottom ripple acts as a stationary wave and mediates energy transfer between the incident and reflected waves (Davies 1982; Mei 1985; Heathershaw 1982). Resonant reflection is maximum when the wavenumber of the bottom corrugations is approximately twice the wavenumber of the incident surface wave. Bragg resonance strongly affects the wave spectrum in continental shelves and coastal regions (Ball 1964), and also modifies the shore-parallel sandbars (Heathershaw & Davies 1985; Elgar *et al.* 2003). Indeed there are many examples of Bragg phenomena in natural settings, e.g. Rotterdam waterway, Cape Cod Bay in Massachusetts, and near numerous shorelines (Couston *et al.* 2015, and references therein).

The objective of this paper is to theoretically and numerically understand in a two-dimensional setting whether Stokes drift is significantly affected by small amplitude undulations on the sea-floor, see figure 1(a) for a schematic diagram. While details would

follow in the rest of the paper, representative results are given in figures 1(b)–1(c). Figure 1(b) shows the standard Stokes drift (in the absence of bottom ripple, the net drift, as expected, is forward), while figure 1(c) reveals that Stokes drift in the presence of bottom ripple changes sign from positive to negative (i.e. undergoes backward motion). Stated otherwise, the presence of bottom ripple can cause a large cancellation of unidirectional drift, and thus cause *particle trapping* in its vicinity.

2. Stokes' waves in a fluid of constant depth

2.1. Governing equation, boundary conditions and a classical solution

We consider an incompressible, inviscid and irrotational fluid inside the domain $\mathcal{B} = \{(x, z) \in \mathbb{R}^2 : -H + \eta_b(x) < z < \eta(x, t)\}$, where H is the mean fluid depth, η denotes the free surface elevation and η_b denotes the bottom topography profile; see figure 1(a). Within the fluid domain \mathcal{B} , the velocity potential $\phi(x, z, t)$ satisfies the Laplace equation

$$\phi_{,xx} + \phi_{,zz} = 0, \quad (2.1)$$

where comma in the subscript denotes partial derivative. Impenetrability condition holds at the bottom boundary $z = -H + \eta_b(x)$:

$$\phi_{,z} - \phi_{,x}\eta_{b,x} = 0, \quad (2.2)$$

which, in case of a flat bottom, simply leads to

$$\phi_{,z} = 0 \quad (2.3)$$

at $z = -H$. The free surface at $z = \eta(x, t)$ evolves in time through the kinematic and dynamic boundary conditions, which can be respectively written as

$$\eta_{,t} + \phi_{,x}\eta_{,x} - \phi_{,z} = 0, \quad (2.4a)$$

$$\phi_{,t} + \frac{1}{2}[(\phi_{,x})^2 + (\phi_{,z})^2] + g\eta = 0, \quad (2.4b)$$

where g denotes gravitational acceleration. The spatio-temporal evolution of periodic, weakly nonlinear water waves can be obtained by solving the governing equation (2.1) and the relevant boundary conditions using perturbation expansions (with wave steepness ' ka ' taken as the small parameter, where a is wave's amplitude and $k \in \mathbb{R}^+$ is its wavenumber). For example, the expressions for η and ϕ for weakly nonlinear surface waves over a fluid of arbitrary (but constant) depth H up to second order (i.e. $\mathcal{O}((ka)^2)$) is given by the classical Stokes' theory (Dingemans 1997; Whitham 2011):

$$\eta(x, t) = a \cos(kx - \omega t) + ka^2 \left[\frac{3 - \tanh^2(kH)}{4 \tanh^3(kH)} \right] \cos(2kx - 2\omega t) + \mathcal{O}((ka)^3), \quad (2.5a)$$

$$\phi(x, z, t) = \frac{a\omega}{k \sinh(kH)} \times \left\{ \cosh[k(z + H)] \sin(kx - \omega t) + ka \frac{3 \cosh[2k(z + H)]}{8 \sinh^3(kH)} \sin(2kx - 2\omega t) \right\} - (ka)^2 \frac{1}{2 \sinh(2kH)} \frac{gt}{k} + \mathcal{O}((ka)^3), \quad (2.5b)$$

where $\omega \in \mathbb{R}$ denotes frequency. Stokes' second order theory reveals steepening of surface wave crests and flattening of troughs for wave propagation over a flat bottom. However, there is yet another second order motion that can arise; this is due to the interactions between first-order motion at the free surface and first order undulations on the sea-bed (Heathershaw & Davies 1985). The latter is known as Bragg reflection – an incident

surface wave resonantly interacts with the bottom ripple of twice its wavenumber to generate a reflected wave.

2.2. Particle trajectories and Stokes drift for two counter-propagating Stokes waves

Let us consider two counter-propagating Stokes waves in a fluid of arbitrary depth H (assumed constant); the wave with surface elevation $\eta_1(x, t)$ travels to the right while that with $\eta_2(x, t)$ propagates to the left:

$$\eta_1 = \epsilon_1 \cos(kx - \omega t) + \epsilon_2 \cos(2kx - 2\omega t), \quad (2.6a)$$

$$\eta_2 = \epsilon_1 R \cos(kx + \omega t + \theta) + \epsilon_2 R^2 \cos(2kx + 2\omega t + \theta), \quad (2.6b)$$

where $\omega > 0$, $\epsilon_1 \equiv a$, $\epsilon_2 \equiv ka^2[3 - \tanh^2(kH)]/[4 \tanh^3(kH)]$, $R \geq 0$ is a parameter and θ is the phase difference between the waves. The potential due to the superposed Stokes' wave $\eta = \eta_1 + \eta_2$ is given by

$$\phi = \phi_1 + \phi_2, \quad (2.7)$$

where ϕ_1 is simply the expression in (2.5b), and ϕ_2 can be obtained by replacing a by Ra and ω by $-\omega$ in (2.5b). The velocity field can be straightforwardly obtained from the velocity potential: $\mathbf{u} \equiv (u, w) = (\phi_{,x}, \phi_{,z})$.

Our primary objective is to obtain the trajectory $(x^{(p)}(t), z^{(p)}(t))$ of a certain tracer particle with initial position (x_0, z_0) . It is more convenient to represent displacements from the initial position: $\boldsymbol{\xi} \equiv (\xi(t), \zeta(t)) \equiv (x^{(p)}(t) - x_0, z^{(p)}(t) - z_0)$. The trajectory can be obtained from the path-line equation:

$$\frac{d\xi}{dt} = u(x^{(p)}, z^{(p)}, t), \quad \frac{d\zeta}{dt} = w(x^{(p)}, z^{(p)}, t). \quad (2.8a,b)$$

The assumption of small excursions from the initial position allows the application of the classical approximation theory (Kundu *et al.* 1990; Constantin & Villari 2008), where $u(x^{(p)}, z^{(p)}, t)$ and $w(x^{(p)}, z^{(p)}, t)$ are Taylor expanded around (x_0, z_0) .

2.2.1. Linear analysis

For linear waves we obtain elliptical trajectory having the following parametric representation:

$$\xi = -\epsilon_1 \frac{\cosh[k(z_o + H)]}{\sinh(kH)} \left\{ \sin(kx_o - \omega t) + R \sin(kx_o + \omega t + \theta) \right\}, \quad (2.9a)$$

$$\zeta = \epsilon_1 \frac{\sinh[k(z_o + H)]}{\sinh(kH)} \left\{ \cos(kx_o - \omega t) + R \cos(kx_o + \omega t + \theta) \right\}. \quad (2.9b)$$

For $R = 0$, we recover the standard parameterization given in Kundu *et al.* (1990). While (2.9a)–(2.9b) is not a surprising outcome, it nevertheless reveals an interesting result; for $R = 1$, the ellipse collapses into a line, which is given by

$$\zeta = -\frac{\tanh[k(z_o + H)]}{\tan(kx_o + \theta/2)} \xi. \quad (2.10)$$

When $kx_o + \theta/2 = 0$, the trajectory is vertical while for $kx_o + \theta/2 = \pm\pi/2$, we obtain a horizontal trajectory. Such linear motions are due to the standing wave pattern generated by the counter-propagating surface waves.

2.2.2. Weakly nonlinear analysis

For weakly nonlinear waves, consideration of $\mathcal{O}((ka)^2)$ terms reveal the celebrated Stokes drift – material parcels drift in the direction of propagation of the wave. Our

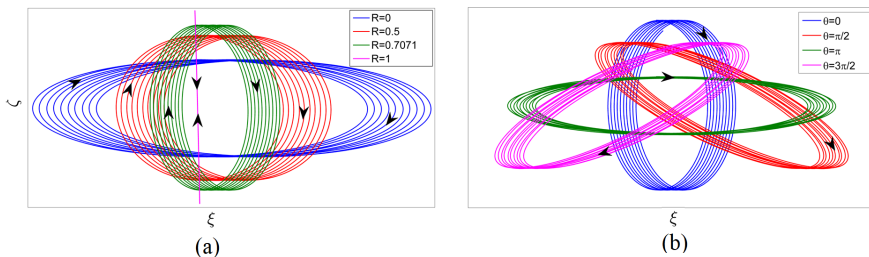


FIGURE 2. Particle trajectories for counter-propagating Stokes waves: (a) $\theta = 0$ and different values of R , and (b) $R = 0.5$ and different values of θ .

objective here is to investigate the drift caused by two counter-propagating Stokes waves η_1 and η_2 . In this regard we follow the usual approach (Kundu *et al.* 1990; Van den Bremer & Breivik 2017; Van Den Bremer *et al.* 2019) to obtain $\mathbf{u}^{(2)} \equiv (u^{(2)}, w^{(2)})$, i.e. \mathbf{u} at $\mathcal{O}((ka)^2)$:

$$u^{(2)} = \frac{\epsilon_1^2 \omega k}{\sinh^2(kH)} \left\{ \cosh^2[k(z_o + H)] \sin^2(kx_o - \omega t) + \sinh^2[k(z_o + H)] \cos^2(kx_o - \omega t) \right\} - \frac{\epsilon_1^2 \omega k R^2}{\sinh^2(kH)} \left\{ \cosh^2[k(z_o + H)] \sin^2(kx_o + \omega t + \theta) + \sinh^2[k(z_o + H)] \cos^2(kx_o + \omega t + \theta) \right\}, \quad (2.11a)$$

$$w^{(2)} = -\epsilon_1^2 \omega k R \frac{\sinh[2k(z_o + H)]}{\sinh^2(kH)} \sin(2\omega t + \theta). \quad (2.11b)$$

We note here in passing that $\mathbf{u}^{(2)} = \boldsymbol{\xi}^{(1)} \cdot \nabla \mathbf{u}^{(1)}|_{(x_o, z_o)}$, i.e. it is a quadratic term resulting from the product of two first order (linear) terms. Time-averaging (2.11a)–(2.11b) over a time-period yields the *generalized* Stokes drift, given by

$$u_{SD} = \epsilon_1^2 \frac{\omega k (1 - R^2)}{2 \sinh^2(kH)} \cosh[2k(z_o + H)]; \quad w_{SD} = 0. \quad (2.12a,b)$$

Substitution of $R = 0$ results in the standard Stokes drift in a fluid of arbitrary depth, first obtained by Ursell (1953). Equations (2.12a,b) reveal that the Stokes drift is *independent* of θ and for $R \in [0, 1]$, the drift velocity *decreases* with increasing R , becoming zero at $R = 1$. This behavior can be visualized graphically in the trajectory plots in figure 2(a), where we chose a particle initially located at $(x_o, z_o) = (0, 0)$. For $R = 1$ case, the particle oscillates along a linear trajectory (vertical in this case), given by (2.10). If $R > 1$, the drift again increases, but in the negative direction. The independence of Stokes drift with θ is evident from figure 2(b).

In summary, this section has revealed in a straight-forward way that two counter-propagating Stokes' waves in a fluid of constant depth (flat bottom) lead to a reduction in the Stokes' drift, which becomes zero when the waves have the same amplitude. The latter is due to the standing wave pattern generated by the counter-propagating Stokes' waves. The drift again increases and its direction reverses when the leftward travelling wave has a higher amplitude. Since Stokes' drift is a time-averaged quantity (over a time-period), the phase difference between the waves does not affect the drift velocity. While there could be numerous situations where one can obtain counter-propagating waves (e.g., those formed by shore-ward propagating waves and waves reflected from the

shore), the situation which we will focus next, and is central to this paper, is Bragg reflection, which occurs when an incident surface wave propagates over a bottom ripple.

3. Bragg resonance and particle trajectories

Nonlinear interaction of an incident surface wave with (small-amplitude) bottom ripple gives rise to a resonant wave, which satisfies the following triad condition:

$$k_i + k_r = k_b, \quad \omega_i + \omega_r = \omega_b,$$

(Liu & Yue 1998). Here the subscripts i , r , and b respectively denote the incident wave, the reflected wave and the bottom ripple. Unlike the classical wave triad formed by three waves, one of the waves is replaced by a stationary bottom ripple in the case of a Bragg triad. Since for the bottom ripple $\omega_b = 0$, it implies $\omega_r = -\omega_i$, i.e. the reflected wave travels in a direction opposite to the incident wave. The dispersion relation for surface waves,

$$\omega^2 - gk \tanh(kH) = 0, \quad (3.1)$$

yields $k_r = k_i$, and hence $k_b = 2k_i$.

To derive the amplitude evolution equations for Bragg resonance, we represent the constituent surface waves in the form $a_i(\tau) \exp[i(k_i x - \omega_i t)] + \text{c.c}$ and $a_r(\tau) \exp[i(k_r x - \omega_r t)] + \text{c.c}$, where c.c denotes complex conjugate, $\tau = \epsilon t$ is the slow time scale, and ϵ is a small parameter. Assuming bottom ripple to have an infinite extent along x , the amplitude evolution equations for Bragg resonance is given by (Raj & Guha 2019):

$$\frac{da_i}{d\tau} = i\lambda \frac{\omega_i}{2g} a_b \bar{a}_r \quad ; \quad \frac{da_r}{d\tau} = i\lambda \frac{\omega_r}{2g} a_b \bar{a}_i, \quad (3.2a,b)$$

where $\lambda = \omega_i \omega_r [\sinh(k_i H) \sinh(k_r H)]^{-1}$, a_b is the complex amplitude of the bottom ripple with overbars denoting the complex conjugates. Equation (3.2a,b) does reveal via the coefficient λ that the effect of Bragg resonance is minimal in the deep water limit, and increases as the water gets shallower. We note here that although (3.2a,b) is simpler and more analytically tractable than the situation with a finite patch of bottom ripple (Davies 1982; Davies & Heathershaw 1984; Mei 1985, for detailed theoretical analyses), it does capture the essential physics of reflected wave generation due to Bragg resonance.

3.1. Numerical implementation of Bragg resonance over a finite patch bottom ripple

Here we intend to numerically simulate the configuration shown in figure 1(a), i.e., Bragg reflection for a finite patch of bottom ripple. The horizontal domain extends from 0 to 2π , and the bottom topography at $z = -H$ is given by the following equation:

$$\eta_b(x) = \begin{cases} a_b \sin(k_b x) & , \pi - \pi/4 \leq x \leq \pi + \pi/4, \\ 0 & , \text{otherwise,} \end{cases} \quad (3.3a,b)$$

where $a_b = 0.1H$ is the amplitude of the bottom ripple, and $k_b H = 2$. For numerical simulation, we employ an in-house code based on the High-order spectral (HOS) method, a highly accurate and efficient numerical method developed by Dommermuth & Yue (1987) for studying wave propagation, wave-wave and wave-topography interactions. Our code is capable of handling multi-layered flows (i.e. both surface and interfacial gravity waves) along with piece-wise constant vorticity in each layer as well, the theoretical and numerical details have been comprehensively reported in a previous paper by our group (Raj & Guha 2019). For the problem relevant to this work, we solve the Laplace equation

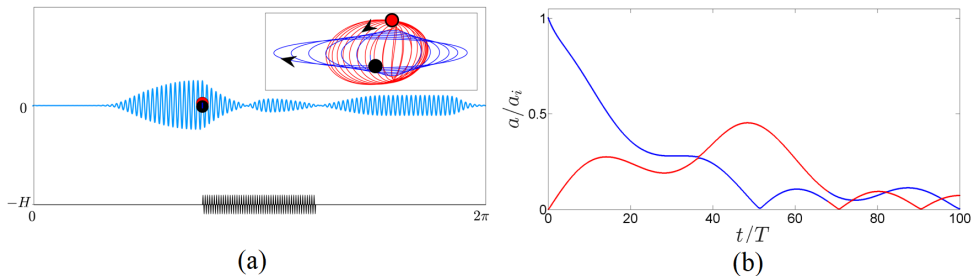


FIGURE 3. (a) The computational domain showing the surface wave profile (light blue) and the bottom ripple (black) during later stages of Bragg resonance. Both surface wave and bottom ripple have been magnified (by different amounts) for visualization. The surface wave shows a complex interference of incident and reflected waves. The black and red filled circles respectively show the initial and final locations of the particle, and has been zoomed in the inset, where the blue curves show forward (clockwise) trajectories and red curves show backward (anti-clockwise) trajectories. (b) Amplitude evolution of the incident (blue) and the reflected (red) waves. Time t has been non-dimensionalized by T , the time-period of the incident wave.

(2.1) along with the boundary conditions (2.2), (2.4a)–(2.4b) using HOS method. The method relies on periodic boundary conditions in the x -direction; periodicity in x allows variables to be expanded as a Fourier series. We have used 1024 Fourier modes, and the order of nonlinearity of the HOS method is kept at 2. Amplification of round-off errors occurs at higher wavenumbers, which needs to be filtered out using a low-pass filter. For time integration, 4-th order Runge-Kutta method has been used. At $t = 0$, a rightward propagating monochromatic incident wave $\eta = a_i \cos(k_i x)$, where $a_i = 0.01H$ and $k_i H = 1$, is added to the free surface. Note that the above choice of the incident wavenumber has been made for satisfying the Bragg resonance condition (since $k_b H = 2$). Furthermore, the wavenumber choice also makes the wave to be of intermediate depth, which is necessary since as mentioned already, Bragg resonance would be minimal in the deep water limit.

Sponge layers have been used (see figure 1(a)) at the horizontal boundaries to prevent interactions between transmitted and reflected waves. A snapshot of the complex wave profile due to Bragg resonance is shown in figure 3(a), along with the trajectory of a tracer parcel located at the free surface. A supplementary movie (Movie 1) has also been provided. Note that while a bottom ripple of infinite extent in x produces a single reflected wave, a finite patch of bottom ripple causes multiple reflections. Figure 3(b) shows that the incident wave (blue color) transfers its energy to the reflected wave (red color) and vice-versa via Bragg resonance; the reflected wave can gain more amplitude than the incident wave during the interaction process. For a tracer parcel, the interface elevation and velocity where the particle is located at a given instant are of key importance. When the local velocity due to the incident wave is higher than that of the reflected wave, the particle undergoes a forward drift (blue curves, denoting clockwise motion in the inset of figure 3(a)). However, when the velocity induced by the reflected wave exceeds that of the incident, the particle traces backwards (red anti-clockwise curves in the inset of figure 3(a)). Such negative drift can be readily observed if $R > 1$ in (2.12a,b). Hence the parcel, which has been transported downstream (i.e. in the direction of propagation of the incident wave) by the incident wave and reached the rippled patch, is prevented to travel any further downstream. Thus the bottom ripple has *trapped* the parcel, or has at least considerably increased its residence time in the rippled zone.

Due to the sponge-layer at the horizontal boundaries, the amplitudes of the incident and reflected waves decay to zero after a long time. In a more realistic scenario, one

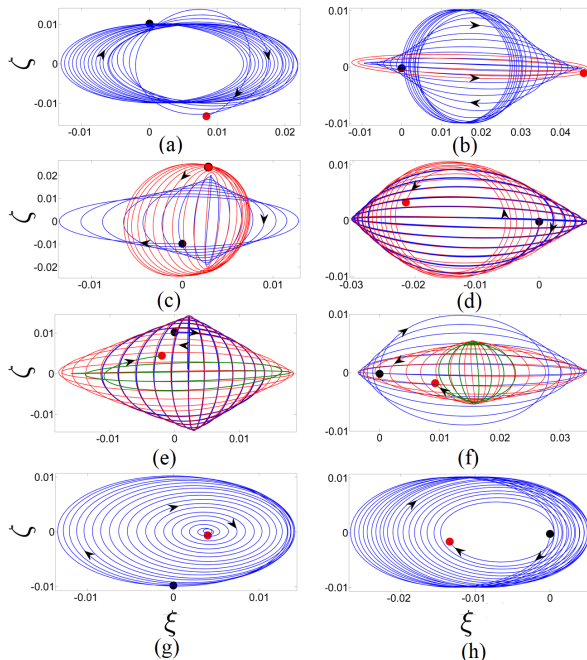


FIGURE 4. Trajectories of tracer parcels at different initial locations as shown in figure 1(a). Blue colored trajectories show forward (clockwise) drift, red shows backward (anti-clockwise) drift, while green shows the next round of forward (clockwise) drift. Black and red filled circles respectively denote initial and final particle positions.

can expect a continuous source of incident wave packets, interacting with the reflected waves that were generated in the past, as well as producing new reflected waves via Bragg resonance. The continuous generation of reflected waves would hinder the downstream propagation of tracer parcels. Hence we expect that the scenario depicted in our simulation would not be fundamentally different from the more realistic case.

3.2. Trajectories of particles at various locations

To understand the fate of particles at different initial locations, we place 8 particles, labelled (a)–(h) on the free surface; see figure 1(a). The particles are evenly distributed in the domain $\pi/2 \leq x \leq 11\pi/8$ (they are at $\pi/8$ distance from each other), and their respective trajectories are depicted in figure 4(a)–4(h). Note that particles (c)–(g) are initially above the bottom ripple, (a)–(b) are upstream while (h) is downstream. Figure 4(a) reveals that the parcel (a) always undergo a forward drift (indicated by blue colored trajectories denoting clockwise circulation), but the drift velocity decreases as soon as the reflected waves pass through it. The effect of the reflected wave becomes more pronounced on parcels (b)–(f), and these parcels undergo anti-clockwise or backward drift (red colored trajectories). The backward drift of parcels (c)–(f) are primarily due to multiple reflections from the finite rippled patch. Green trajectories for parcels (e)–(f) denote the next sequence of forward drift, and occurs when the incident wave again dominates over the reflected. Parcels (g)–(h) undergo forward drift due to the transmitted wave, but their drift velocities decrease with time. In summary, all parcels existing in the vicinity of the rippled patch experience a drastic change in their otherwise forward drift, the rippled patch acts as an effective, non-surface-invasive particle trap.

4. Summary and Conclusion

The seminal work of Stokes showed that surface waves cause mass transport; particles undergo a slow drift in the direction of propagation of the waves. This theory is central for understanding how material parcels, e.g. pollutants, sediments, plankton, etc., are transported in aquatic environments. While there exists a vast literature on Stokes drift, to the best of our knowledge, the effect of small-amplitude sea-floor corrugations on the drift velocity has not been explored previously.

In this paper we have first considered the simplest setting of two counter-propagating Stokes' waves (with amplitudes a and Ra) in a fluid of constant depth, and have analytically demonstrated that Stokes drift diminishes as R increases (for $0 \leq R \leq 1$), and becomes zero when $R = 1$. Furthermore for $R > 1$, the drift again increases but in the negative direction. Counter-propagating waves may arise when a surface wave travels over a corrugated bottom topography; nonlinear resonant interaction between an incident surface wave and a small amplitude rippled bottom gives rise to a reflected wave. The theoretical underpinnings of this process – the Bragg resonance – has been described next; it has been shown that an incident wave (k_i, ω_i) , mediated by a bottom ripple of wavenumber $k_b = 2k_i$, transfers energy (and vice versa) to a reflected wave $(k_r, \omega_r) = (k_i, -\omega_i)$. The energy transfer is more pronounced in shallower regions of the oceans such as littoral zones. Finally using HOS method, we have numerically investigated the effect of a finite patch of bottom ripple on Stokes drift. When the incident wave is rightward propagating and the bottom is flat, we expect a unidirectional Stokes drift (rightward in this case) with clockwise circulating particle trajectories. The rippled patch, however, leads to Bragg reflection, rendering the free surface a complex interference of incident and reflected waves. When the induced velocity due to the reflected waves is stronger than the incident, the drift is backward (leftward), and the particle trajectories have an anti-clockwise circulation. This is analogous to $R > 1$ case in our theoretical analysis with Stokes waves. We have demonstrated the reversal of Stokes drift by studying trajectories of multiple parcels placed on the free surface above the patch. Hence we conclude that the rippled patch acts as a non-surface-invasive particle trap.

While we demonstrated this trapping mechanism for a monochromatic incident wave, in real ocean scenarios an incident wave-group contains a spectrum of frequencies and is composed of many (linearly or nonlinearly) superposed wave components. Motivated by wave energy harvesting and coastal protection applications, Elandt *et al.* (2014) studied Bragg resonance (specifically, surface wave lensing) using broadband spectrum of incident waves and polychromatic topography. Complexity does arise because of super/sub-harmonic generations, quartet and higher-order Bragg resonances, however the underlying mechanism of lensing of monochromatic and broadband waves is similar. Hence we expect that in realistic scenarios, a properly designed artificial patch of bottom ripple can serve multiple purposes – from wave energy harvesting to pollutant trapping. One application of our work could be mitigating microplastic pollution, which is a growing concern and a severe threat to the marine environment. Studies suggest that mechanical degradation of plastics occur in coastal areas, leading to microplastics, which then makes its onward journey into the deep sea (Chubarenko *et al.* 2018). Topographic interactions are inevitable in littoral zones, and our study has revealed that small amplitude sea-floor corrugations, which might seem unimportant, can significantly affect the trajectories of microplastics and other pollutants. Hence high resolution coastal bathymetry map needs to be included for predicting pollutant pathways.

Acknowledgement: The authors thank G. Saranraj for carefully reading the manuscript, and providing useful comments and suggestions.

REFERENCES

- BALL, F. K. 1964 Energy transfer between external and internal gravity waves. *J. Fluid Mech.* **19**, 465–478.
- VAN DEN BREMER, T. S. & BREIVIK, Ø. 2017 Stokes drift. *Philos. Trans. R. Soc. A* **376** (2111), 20170104.
- CHUBARENKO, I., ESIUKOVA, E., BAGAEV, A., ISACHENKO, I., DEMCHENKO, N., ZOBKOV, M., EFIMOVA, I., BAGAEVA, M. & KHATMULLINA, L. 2018 Behavior of microplastics in coastal zones. In *Microplastic Contamination in Aquatic Environments*, pp. 175–223. Elsevier.
- CONSTANTIN, A. & VILLARI, G. 2008 Particle trajectories in linear water waves. *J. Math. Fluid Mech.* **10** (1), 1–18.
- COUSTON, L-A., GUO, Q., CHAMANZAR, M. & ALAM, M-R. 2015 Fabry-Perot resonance of water waves. *Phys. Rev. E* **92**, 043015.
- DAVIES, A. G. 1982 The reflection of wave energy by undulations on the seabed. *Dynam. Atmos. Oceans* **6** (4), 207–232.
- DAVIES, A. G. & HEATHERSHAW, A. D. 1984 Surface-wave propagation over sinusoidally varying topography. *J. Fluid Mech.* **144**, 419–443.
- DINGEMANS, M. W. 1997 *Water wave propagation over uneven bottoms*, , vol. 13. World Scientific.
- DOMMERMUTH, D. G. & YUE, D. K. P. 1987 A high-order spectral method for the study of nonlinear gravity waves. *J. Fluid Mech.* **184**, 267–288.
- ELANDT, R. B., SHAKERI, M. & ALAM, M-R. 2014 Surface gravity-wave lensing. *Phys. Rev. E* **89** (2), 023012.
- ELGAR, S., RAUBENHEIMER, B. & HERBERS, T.H.C. 2003 Bragg reflection of ocean waves from sandbars. *Geophys. Res. Lett.* **30** (1).
- HEATHERSHAW, A.D. & DAVIES, A.G. 1985 Resonant wave reflection by transverse bedforms and its relation to beaches and offshore bars. *Mar. Geol.* **62** (3-4), 321–338.
- HEATHERSHAW, A. D. 1982 Seabed-wave resonance and sand bar growth. *Nature* **296** (5855), 343.
- KUNDU, P. K., COHEN, I. & DOWLING, D. 1990 Fluid mechanics. 1990. *Academic Press* **77**, 108.
- LIU, Y. & YUE, D. K. P. 1998 On generalized bragg scattering of surface waves by bottom ripples. *J. Fluid Mech.* **356**, 297–326.
- MCWILLIAMS, J.C. & RESTREPO, J. M. 1999 The wave-driven ocean circulation. *J. Phys. Oceanogr.* **29** (10), 2523–2540.
- MEI, C. C. 1985 Resonant reflection of surface water waves by periodic sandbars. *J. Fluid Mech.* **152**, 315–335.
- RAJ, R. & GUHA, A. 2019 On bragg resonances and wave triad interactions in two-layered shear flows. *J. Fluid Mech.* **867**, 482515.
- SANTAMARIA, F., BOFFETTA, G., AFONSO, M. M., MAZZINO, A., ONORATO, M. & PUGLIESE, D. 2013 Stokes drift for inertial particles transported by water waves. *Europhys. Lett.* **102** (1), 14003.
- VAN SEBILLE, E., ALIANI, S., LAW, K.L., MAXIMENKO, N., ALSINA, J., BAGAEV, A., BERGMANN, M., CHAPRON, B., CHUBARENKO, I., CZAR, A., DELANDMETER, P., EGGER, M., FOX-KEMPER, B., GARABA, S.P., GODDIJN-MURPHY, L., HARDESTY, D., HOFFMAN, M.J., ISOBE, A., JONGEDIJK, C., KAANDORP, M., KHATMULLINA, L., KOELMANS, A.A., KUKULKA, T., LAUFKTTTER, C., LEBRETON, L., LOBELLE, D., MAES, C., MARTINEZ-VICENTE, V., MAQUEDA, M.A.M., POULAIN-ZARCOS, M., RODRIGUEZ, E., RYAN, P.G., SHANKS, A., SHIM, W.J., SUARIA, G., THIEL, M., VAN DEN BREMER, T. & WICHMANN, D. 2020 The physical oceanography of the transport of floating marine debris. *Environ. Res. Lett.* .
- STOKES, G. G. 1847 On the theory of oscillatory waves. *Trans. Camb. Philos. Soc.* **8**, 441.
- URSELL, F. 1953 The long-wave paradox in the theory of gravity waves. In *Math. Proc. Camb. Philos. Soc.* , vol. 49, pp. 685–694. Cambridge University Press.
- VAN DEN BREMER, T. S., WHITTAKER, C., CALVERT, R., RABY, A. & TAYLOR, P. H. 2019 Experimental study of particle trajectories below deep-water surface gravity wave groups. *J. Fluid Mech.* **879**, 168–186.
- WHITHAM, G. B. 2011 *Linear and nonlinear waves*, , vol. 42. John Wiley & Sons.